Optical lattice for a tripodlike atomic level structure

Piotr Kubala,[1] Jakub Zakrzewski [●],[1,2] and Mateusz Łącki [●][1,*]

[1]*Institute of Theoretical Physics, Jagiellonian University, Łojasiewicza 11, 30-348 Kraków, Poland*

[2]*Mark Kac Complex Systems Research Center, Jagiellonian University in Krakow, Łojasiewicza 11, 30-348 Kraków, Poland*

Standard optical potentials use an off-resonant laser standing-wave-induced ac Stark shift. In a recent development [Łącki *et al.*, Phys. Rev. Lett. **117**, 233001 (2016)] a three-level scheme in a Λ configuration coupled coherently by resonant laser fields was introduced, leading to an effective lattice with subwavelength potential peaks. Here, as an extension of that work, a four-level atomic setup in the tripod configuration is used to create spin-$\frac{1}{2}$-like two-dimensional dark space with one-dimensional motion and the presence of external gauge fields. Most interestingly for possible applications, the lifetime for a dark subspace motion is up to two orders of magnitude longer than for a similar Λ system. The model is quite flexible, leading to lattices with significant nearest, next-nearest, or next-to-next-nearest hopping amplitudes J_1, J_2, and J_3 offering intriguing possibilities to study, e.g., frustrated systems. The characteristic Wannier functions lead also to a type of intersite interaction not realizable in typical optical lattices.

I. INTRODUCTION

Optical potentials using a Stark shift induced by far-detuned laser standing waves have enabled implementation of discrete lattice models [1] linking ultracold atomic physics with condensed matter physics or rather enriching the latter with bosonic systems such as the Bose-Hubbard model. The experimental demonstration of a quantum phase transition between the superfluid and Mott insulating phases [2] was followed by intensive investigations in different, more complex schemes [3–5] involving spinor lattice gases, long-range interactions, disordered systems, or an implementation of topological insulators.

Standing-wave optical potentials have proved to be very versatile, allowing one to create, typically with the application of additional Raman lasers, interesting coupling between sites, e.g., leading to the construction of artificial gauge fields or spin-orbit coupling as reviewed in [5]. The atomic ground-state sublevels could serve as an additional synthetic dimension [6–8], allowing, e.g., the extension of Hall physics to four dimensions [9]. Still, the standing-wave optical potential has some drawbacks. The typical $\cos^2(k_L x)$ spatial dependence (with k_L being the laser light wave vector) leads to the dominance of nearest-neighbor tunneling over hops involving separated sites. Similarly, on-site interactions dominate over intersite terms, making investigations of interaction-related physics for spinless fermions in optical lattices difficult.

Recently, an alternative scheme for creating optical potentials has been proposed [10,11]. It relies on a *resonant* dipole coupling of three atomic levels with the position-dependent Rabi frequencies involving a common atomic excited state. This differs from the standard approach where two-photon resonant lasers are far detuned from a single-photon transition

[12,13]. The resulting Λ system is characterized by a position-dependent dark state. The dynamics of atoms constrained to the dark state is that of a particle moving in the presence of a scalar potential which features evenly spaced subwavelength peaks. Early ^{171}Yb experiments [14,15] confirmed the expected band structure, but the system lifetimes were, disappointingly, at least one order of magnitude lower than for ac Stark potentials.

In this work we present the tripod system [16,17], with four resonantly coupled levels, which is an interesting extension of the Λ system. It features two degenerate dark states implementing spin-$\frac{1}{2}$-like physics providing at the same time a possible realization of spin-orbit coupling in a one-dimensional lattice supplementing the existing schemes [18,19]. In Sec. II we adapt the derivation of the Λ system dark-state description to the tripod scheme. In Sec. III we detail the resulting periodic spin-$\frac{1}{2}$-like model for the movement of the particle in the gauge field and discuss the Bloch theory including lifetime computation of the dark-state bands. The tight-binding description of atoms populating low-lying bands is discussed in Sec. IV. As it turns out, the model leads, in a natural way, to a quite peculiar extended Hubbard model with significant hopping not only to the nearest-neighbor (NN) sites but also to the next-nearest neighbors (NNNs) and to next-to-next-nearest neighbors (NNNNs). Such a highly interesting and unusual property is due to the shape of the Wannier basis functions corresponding to the nonstandard lattice experienced by the atoms. This opens up the possibility of frustration-related studies in the model. A summary is given and future perspectives involving the study of interacting particles are discussed in Sec. V.

II. HAMILTONIAN

We consider a gas of ultracold atoms whose motion is restricted to one dimension, for example, by a strong external optical potential of the form $V(y, z) = m_a \omega^2 (y^2 + z^2)/2$. The

_____

*mateusz.lacki@uj.edu.pl

atoms populate three ground-state configuration atomic states $|g_1\rangle$, $|g_2\rangle$, and $|g_3\rangle$ that are coupled to an excited state $|e\rangle$. The dipole coupling of each of $|g_i\rangle$ to $|e\rangle$ is characterized by a Rabi frequency $\Omega_i(x)$. The wavelength of the three lasers is assumed to be equal to λ_L. In a rotating frame, after neglecting rapidly oscillating terms, the Hamiltonian of the system considered reads

$$H = -\frac{\hbar^2}{2m_a}\frac{\partial^2}{\partial x^2} + H_a(x), \qquad (1)$$

where m_a is the atomic mass and

$$H_a(x) = \begin{pmatrix} -\Delta - \frac{i\Gamma_e}{2} & \Omega_1^*(x) & \Omega_2^*(x) & \Omega_3^*(x) \\ \Omega_1(x) & 0 & 0 & 0 \\ \Omega_2(x) & 0 & 0 & 0 \\ \Omega_3(x) & 0 & 0 & 0 \end{pmatrix}. \qquad (2)$$

Here Δ is a possible common detuning of all three lasers and Γ_e is spontaneous emission rate of the excited state. We consider Rabi frequencies of the form

$$\begin{aligned} \Omega_1(x) &= \Omega_1 \sin(k_L x), \\ \Omega_2(x) &= \Omega_2 \sin(k_L x + a), \qquad (3) \\ \Omega_3(x) &= \Omega_3, \end{aligned}$$

where $k_L = 2\pi/\lambda_L$. The λ_L periodicity defines a natural energy scale: the recoil energy equal to $E_R = \hbar^2 k_L^2 / 2m_a$.

The matrix $H_a(x)$ in Eq. (2), for $\Gamma_e \neq 0$, is non-Hermitian. It is diagonalized by finding a biorthogonal set of right and left eigenvectors. When using bra-ket notation, the bra vector always refers to a proper left eigenvector, a part of the biorthogonal set. There exist two linearly independent right eigenvectors $|D_1(x)\rangle$ and $|D_2(x)\rangle$ corresponding to energy $E(x) = 0$, two dark states. They are of the form

$$|D_i(x)\rangle = \sum_{n=1}^{3} u_{i,n}|g_i\rangle, \quad \mathbf{\Omega}(x) \perp \mathbf{u}_i \qquad (4)$$

and are not affected by value of Δ or Γ_e.

The Hamiltonian matrix (2) has also two (right) bright states $|B_\pm(x)\rangle$ with energies

$$E_\pm(x) = -\tilde{\Delta}/2 \pm \sqrt{(\tilde{\Delta}/2)^2 + \|\mathbf{\Omega}(x)\|^2}, \qquad (5)$$

where $\tilde{\Delta} = \Delta + i\Gamma/2$. These states read

$$|B_\pm(x)\rangle = \mathcal{N}_\pm(x)\left(E_\pm(x)|e\rangle + \sum_{i=1}^{3}\Omega_i(x)|g_i\rangle\right), \qquad (6)$$

where

$$\begin{aligned} \mathcal{N}_\pm(x) &= \frac{1}{\sqrt{[E_\pm(x)]^2 + \|\mathbf{\Omega}\|^2}}, \\ \|\mathbf{\Omega}\| &= \sqrt{|\Omega_1(x)|^2 + |\Omega_2(x)|^2 + |\Omega_3(x)|^2} \qquad (7) \end{aligned}$$

are the normalization factors. The left eigenvectors, which together with (6) form a biorthonormal set, are given by

$$\langle B_\pm(x)| = \mathcal{N}_\pm(x)\left(E_\pm(x)\langle e| + \sum_{i=1}^{3}\Omega_i^*(x)\langle g_i|\right). \qquad (8)$$
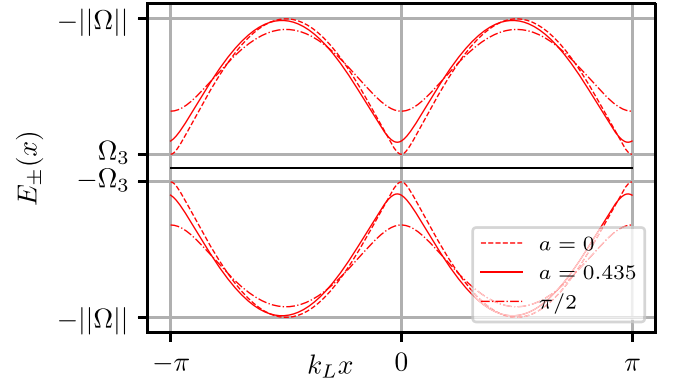

FIG. 1. Diagonal energies of bright channels $E_+(x) > 0$ and $E_-(x) < 0$ for $\Omega_1:\Omega_2:\Omega_3 = 5000:2000:500$. For $a \in \{0, \pi/2\}$ the $E_+(x)$ has a minimum for $x = 0$.

For $\Gamma_e \neq 0$ the states $|B_\pm(x)\rangle$ undergo a spontaneous emission with a rate comparable to that of an excited state $|e\rangle$. In this work we are interested in the case when atoms populate primarily the stable channels $|D_1(x)\rangle$ and $D_2(x)\rangle$ and the energy scale set by Ω_i dominates the kinetic energy of atoms. This also ensures that a phenomenological description of losses from largely unpopulated $|e\rangle$ via $i\Gamma_e$ is justified, $\Gamma_e \ll \|\mathbf{\Omega}\|$.[1]

The gap ΔE between the dark- and the bright-state channels, for $\Delta = 0$, is given by $\min E_+(x)$. For $a = 0$ we have $\Delta E = |\Omega_3|$. For $a > 0$ the gap ΔE increases until $a = \pi/2$, where $\Delta E = \min\{\sqrt{\Omega_3^2 + \Omega_2^2}, \sqrt{\Omega_3^2 + \Omega_1^2}\}$. The dependence of $E_\pm$ on x for a few selected values of a is shown in Fig. 1.

It is worth stressing that we focus on noninteracting bosons or the physics of ultracold spinless fermions, where direct collisions are suppressed. If this were not the case one may wonder whether the collision of two atoms in the dark state may not lead to one particle in each bright state as $E_+(x) + E_-(x) = -\tilde{\Delta}$. We leave this question open for the interacting case study; here we mention that the process may be suppressed by taking a sufficient detuning Δ still in the limit $\Delta \lesssim\gtrsim \|\mathbf{\Omega}\|$.

The Hamiltonian (1) may be addressed using a Born-Oppenheimer type of transformation [10,16] applying

$$\mathcal{B}(x) = \{|D_1(x)\rangle, |D_2(x)\rangle, |B_+(x)\rangle, |B_-(x)\rangle\} \qquad (9)$$

as a position-dependent basis. Writing an arbitrary wave function in this basis as

$$\begin{aligned} |\psi(x)\rangle &= d_1(x)|D_1(x)\rangle + d_2(x)|D_2(x)\rangle \\ &+ b_-(x)|B_-(x)\rangle + b_+(x)|B_+(x)\rangle \qquad (10) \end{aligned}$$

yields the Hamiltonian matrix

$$H_\mathcal{B} = \frac{[P - A(x)]^2}{2m_a} + \text{diag}[0, 0, E_+(x), E_-(x)] \qquad (11)$$

---

[1]In general, the more complete treatment of losses would be by the Lindblad master equation approach.

or

$$H_{\mathcal{B}} = \frac{1}{2m_a}[P^2 - 2A(x)P + \Phi(x)]$$
$$+ \text{diag}[0, 0, E_+(x), E_-(x)]. \quad (12)$$

The $H_{\mathcal{B}}$ now acts on vectors of the form

$$\psi(x) \equiv \begin{pmatrix} d_1(x) \\ d_2(x) \\ b_+(x) \\ b_-(x) \end{pmatrix}. \quad (13)$$

The operator $P = -i\hbar\partial_x \otimes \mathbf{1}_4$. The $A(x)$ is given by

$$A_{MN}(x) = i\hbar\langle M(x)|\partial_x|N(x)\rangle, \quad M(x), N(x) \in \mathcal{B}(x) \quad (14)$$

and

$$\Phi(x) = A(x)^2 + i\hbar\partial_x A(x). \quad (15)$$

A. Dark-state subspace

The large diagonal terms $E_-(x)$ and $E_+(x)$ in Eq. (12) allow for the separation of the dark-state physics in the Hamiltonian (12) by the following dark-state projection:

$$H_2 = QH_{\mathcal{B}}Q, \quad Q = |D_1(x)\rangle\langle D_1(x)| + |D_2(x)\rangle\langle D_2(x)|. \quad (16)$$

This will be evident from the upcoming numerical analysis.

The states $|D_1(x)\rangle$ and $|D_2(x)\rangle$ are energy degenerate and thus not uniquely defined. Different choices of basis lead to an equivalent description of the model. We favor those leading to simple, well-behaved, and intuitive potentials $A(x)$. We consider only λ_L-periodic $|D_i(x)\rangle$. We also opt to work with $|D_i(x)\rangle$ with real coefficients, which automatically implies $A_{11}(x) = A_{22}(x) = 0$.

Let us take

$$|D_1(x)\rangle \propto |\xi\rangle \times \boldsymbol{\Omega}(x) \quad (17)$$

and

$$|D_2(x)\rangle \propto |D_1(x)\rangle \times \boldsymbol{\Omega}(x). \quad (18)$$

This ensures their mutual orthogonality and by Eq. (4) such vectors are indeed dark. The vector $|\xi\rangle$ cannot be parallel to $\boldsymbol{\Omega}(x)$ but otherwise can be arbitrary. We choose

$$|\xi\rangle = \Omega_1|g_1\rangle + \Omega_2|g_2\rangle. \quad (19)$$

We will later discuss the advantages of the above choice for $|\xi\rangle$, namely, good analytic properties in the limit $a \to 0$. Using Eq. (19) we find

$$|D_1(x)\rangle = N_1(x)\begin{pmatrix} \Omega_2\Omega_3 \\ -\Omega_1\Omega_3 \\ \Omega_1\Omega_2[\sin(a + k_Lx) - \sin(k_Lx)] \end{pmatrix} \quad (20)$$

and

$$|D_2(x)\rangle = N_2(x)\begin{pmatrix} \Omega_1[\Omega_2^2 f(k_Lx) + \Omega_3^2] \\ \Omega_2[\Omega_1^2 f(\pi/2 + k_Lx - a/2) + \Omega_3^2] \\ -\Omega_3[\Omega_2^2 \sin(a + k_Lx) + \Omega_1^2 \sin(k_Lx)] \end{pmatrix}, \quad (21)$$

where

$$f(y) = \sin(a + y)[\sin(a + y) - \sin(y)]. \quad (22)$$

When $a = 0$ the state $|D_1(x)\rangle$ becomes position independent

$$|D_1(x)\rangle = \frac{\Omega_2}{\sqrt{\Omega_1^2 + \Omega_2^2}}|g_1\rangle - \frac{\Omega_1}{\sqrt{\Omega_1^2 + \Omega_2^2}}|g_2\rangle \quad (23)$$

and

$$D_2(x) = N_2(x)\big[\Omega_1\Omega_3|g_1\rangle + \Omega_2\Omega_3|g_2\rangle$$
$$- (\Omega_1^2 + \Omega_2^2)\sin(k_Lx)|g_3\rangle\big]. \quad (24)$$

The latter can be written as

$$|D_2(x)\rangle = \frac{1}{\sqrt{\Omega_p^2 + \Omega_c^2}}[\Omega_p|a\rangle - \Omega_c\sin(k_Lx)|g_3\rangle], \quad (25)$$

where $|a\rangle = \cos\beta|g_1\rangle + \sin\beta|g_2\rangle$, $\tan\beta = \Omega_2/\Omega_1$, $\Omega_c = \sqrt{\Omega_1^2 + \Omega_2^2}$, and $\Omega_p = \Omega_3$. The above form is formally identical to the form of a single dark state in the Λ system configuration [10].

At this point let us briefly comment on why $|\xi\rangle = \Omega_1|g_1\rangle + \Omega_2|g_2\rangle$ is a good choice for the vector that generates $|D_1(x)\rangle$ and $|D_2(x)\rangle$ by Eqs. (17) and (18). Let us consider, for example, $|\xi\rangle = |g_3\rangle$. It leads to

$$|D_1(x)\rangle \sim -\Omega_2\sin(k_Lx + a)|g_1\rangle + \Omega_1\sin k_Lx|g_2\rangle, \quad (26)$$

$$|D_2(x)\rangle \sim \Omega_1\Omega_3\sin k_Lx|g_1\rangle + \Omega_2\Omega_3\sin(k_Lx + a)|g_2\rangle$$
$$- \big[\Omega_1^2\sin^2 k_Lx + \Omega_2^2\sin^2(k_Lx + a)\big]|g_3\rangle, \quad (27)$$

which is apparently analytically simpler than the previous results (20) and (21). In fact, it gives simple analytic calculations of coefficients of $A(x)$ and $A^2(x)$ (see Appendix B). However, the limit $a \to 0$ agrees with Eq. (23) only up to a sign, namely, both $|g_1\rangle$ and $|g_2\rangle$ components flip their signs when $k_Lx = n\pi$; n is an integer making them only piecewise constant and, in particular, discontinuous. For that reason, the derivatives in the definition of $A(x)$ [Eq. (14)] are ill-defined as $a \to 0$.

B. Gauge potentials

Having chosen the dark-state basis $|D_i(x)\rangle$ [Eqs. (20) and (21)], one finds the gauge potential $A(x)$ with Eq. (14). For the dark-state projected Hamiltonian H_2 one restricts $A(x)$ and $A^2(x)$ to the upper left 2×2 block. The coefficients $A_{ij}(x)$ for $i, j < 3$ clearly do not depend on the choice of the bright-state phase, as evident from (14). The same holds for $(A^2)_{ij}(x)$ [16]:

$$(A^2)_{ij}(x) = -\hbar^2\sum_{M(x)\in\mathcal{B}(x)}\langle D_i|M'(x)\rangle\langle M|D_j'(x)\rangle$$
$$= \hbar^2\langle D_i'(x)|D_j'(x)\rangle. \quad (28)$$

Let us first consider a special case of $a = 0$. With the position-independent $|D_1(x)\rangle$ and $|D_2(x)\rangle$ given by (24), the coefficients of 2×2 projections of $A(x)$ and $A^2(x)$ included in (16) are all zero except for the $(A^2)_{22}(x)$, which is equal to

$$(A^2)_{22}(x) = \left(\frac{\epsilon\cos k_Lx}{\epsilon^2 + \sin^2 k_Lx}\right)^2, \quad (29)$$

with $\epsilon = \Omega_3/\sqrt{\Omega_1^2 + \Omega_2^2} = \Omega_p/\Omega_c$, in analogy to the Λ system. The Hamiltonian H_2 is then a direct sum of two decoupled D_1 and D_2 channels. The Hamiltonian (12) for the particle in the D_1 channel is that of a freely moving particle

$$H = -\frac{\hbar^2}{2m}\frac{d^2}{dx^2}, \qquad (30)$$

with running-wave eigenfunctions of the form $d_1(x) = \exp(iqx)$. The Hamiltonian H_2 for the particle in the D_2 channel reduces to the movement in the scalar potential given by $(A^2)_{22}(x)$:

$$H = -\frac{\hbar^2}{2m}\frac{d^2}{dx^2} + (A^2)_{22}(x). \qquad (31)$$

The above potential, given by (29), is precisely the subwavelength comb potential which appears for the Λ system construction [10]. It is shown in Fig. 2(a).

For $a \neq 0$ the coefficients $A_{12}(x)$ and $(A^2)_{12}(x)$ are nonzero and the two channels D_1 and D_2 are coupled. Figure 2(b) shows the spatial dependence of $A(x)$ and $A^2(x)$ for a small $a = 0.05$ value [for that a value, the $(A^2)_{22}(x)$ resembles that for $a = 0$]. The potentials change for a larger value of a as shown in Figs. 2(c) and 2(d) for $a = 0.435$. The potentials $(A^2)_{11}$ and $(A^2)_{22}$ are in the form of a comb, with $(A^2)_{22}$ being much larger than $(A^2)_{11}$ [the remnant of vanishing $(A^2)_{11}$ in the limiting case $a = 0$]. This is also evident from Fig. 2(e), which shows the maximum height of $(A^2)_{11}$ and $(A^2)_{22}$ as a function of a. All the above potentials are clearly $\lambda_L/2$ periodic, implying that the dark-state-only model H_2 has period $\lambda_L/2$, half of the period of the full model H.

The potential shapes depend obviously on the choice of the basis in the dark subspace. In Appendix A this issue is discussed further.

III. BAND STRUCTURE

A. General considerations

We discuss the band structure of the full model (1). In numerical calculations we work directly with the full Hamiltonian (1). The Born-Oppenheimer decomposition into dark and bright states, and in particular Hamiltonian H_2 in Eq. (16) is instrumental for the interpretation of the results.

We look for the quasiperiodic Bloch eigenstates of the λ_L-periodic model (1) directly in the $|g_i\rangle$ and $|e\rangle$ basis:

$$B_q(x) = e^{iqx}\left(\sum_{i=1}^{3} b_{g_i}(x)|g_i\rangle + b_e(x)|e\rangle\right) \qquad (32)$$

$$\equiv e^{iqx}[b_{g_1}(x), b_{g_2}(x), b_{g_3}(x), b_e(x)]^T. \qquad (33)$$

The period of the Hamiltonian and the Bloch theory guarantee that $b_*(x)$ are λ_L-periodic functions and q is the quasimomentum $q \in \mathrm{BZ}_1 = [-\pi/\lambda_L, \pi/\lambda_L)$, where BZ_1 is the Brillouin zone. Looking at Eq. (1) and the spatial dependence of Ω_i, one finds an extra parity symmetry: The coefficients b_{g_i} and b_e are actually all $\lambda_L/2$ periodic or $\lambda_L/2$ antiperiodic, and if b_{g_1} and b_{g_2} are $\lambda_L/2$ periodic then b_e and b_{g_3} are $\lambda_L/2$ antiperiodic and vice versa.
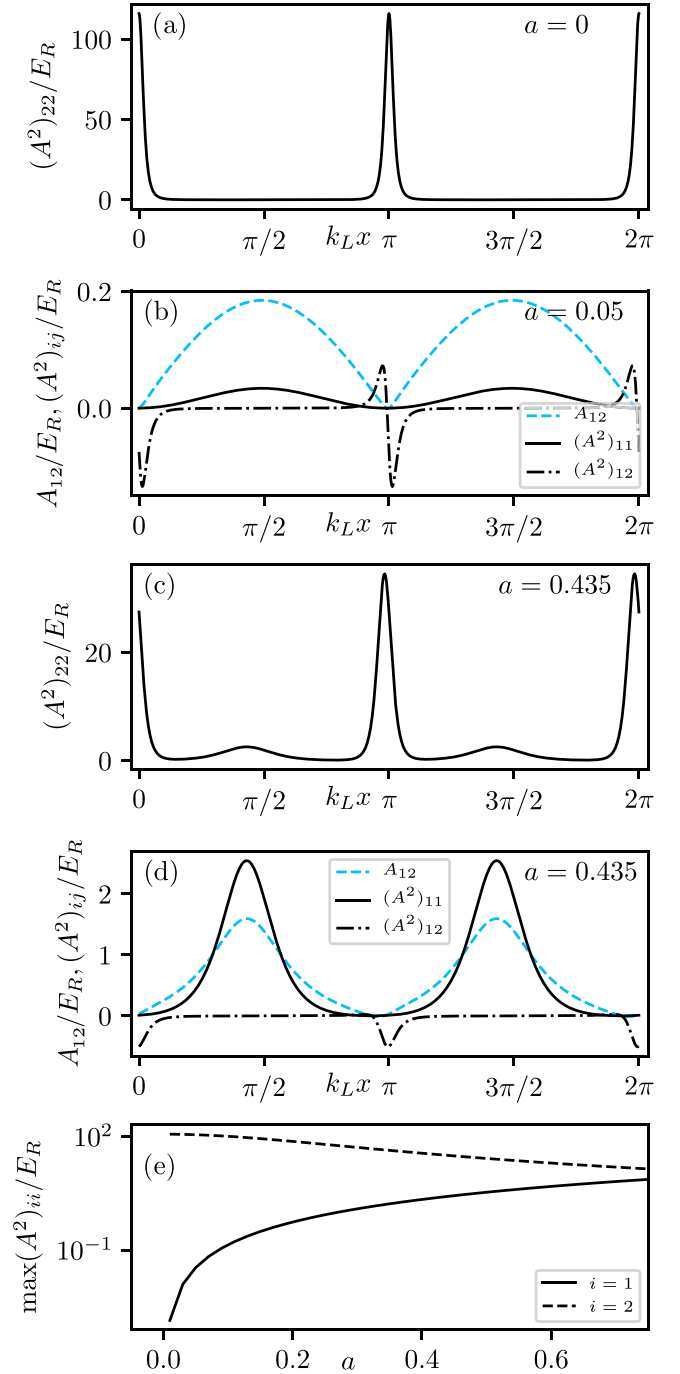

FIG. 2. Spatial dependence of elements of matrices $A(x)$ and $A^2(x)$ describing the couplings within the dark-state subspace for $\Omega_1:\Omega_2:\Omega_3 = 50:20:5$. The value of the phase shift a is indicated in each of the panels. (a) Limiting case of $a = 0$ for $(A^2)_{22}(x)$ [see also Eq. (29)]. (b) Coefficients $A_{12}(x)$, $(A^2)_{11}$, and $(A^2)_{12}(x)$ for a small but nonzero $a = 0.05$. The coefficient $(A^2)_{22}(x)$ for this a is similar to that in (a). (c) Coefficient $(A^2)_{22}(x)$ for a larger $a = 0.435$. (d) Smaller coefficients $A_{12}(x)$, $(A^2)_{11}$, and $(A^2)_{12}(x)$. (e) Dependence of the peak height of $(A^2)_{11}(x)$ and $(A^2)_{22}(x)$ on the phase a.

For the numerical formulation of the eigenproblem for the Hamiltonian (1), the Fourier series expansion of $b_*(x)$ is used. It puts the Hamiltonian H in a sparse matrix form, which is
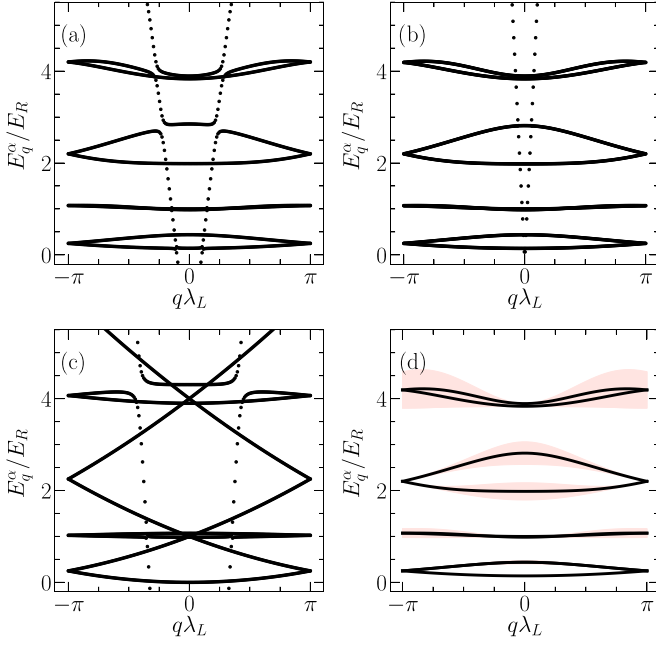
FIG. 3. Band structure of the model (1) for $\Omega_1:\Omega_2:\Omega_3 = 50:20:5$. (a) Spectrum for $\Omega_1 = 1000E_R$ and $a = 0.435$. (b) Spectrum for $\Omega_1 = 5000E_R$ and $a = 0.435$. (c) Dark-state-only limit of the band structure for $\Omega_1 = 5000E_R$ and $a = 0$ ($\Gamma_e = 0$). (d) Band structure for $\Gamma_e = 1000E_R$ and $\Omega_1 = 5000E_R$. The black line within bands shows the $\mathrm{Re}E_q^\alpha$ curves and the red region is given by the $\mathrm{Re}E_q^\alpha \pm 50\,\mathrm{Im}E_q^\alpha$ curves, denoting q-dependent losses due to spontaneous emission. For clarity, the bright-state eigenvalues have been removed from this panel.

diagonalized using standard numerical packages.[2] The different eigenvalues E_q^α are indexed by α for each value of $q \in \mathrm{BZ}_1$.

Consider first the $\Gamma_e = 0$ case; the corresponding band structure obtained for some particular values of Ω_i is depicted in Fig. 3. When $\|\mathbf{\Omega}\|$ dominates other energy scales, the full spectrum contains energy levels that can be traced back to E_- bright states, E_+ bright states, and dark states D_1 and D_2, effectively described by Eq. (16).

Figure 3(a) shows the section of the band structure at low energies above zero that feature a series of bands and two nearly vertical lines of eigenvalues intersecting them. We identify the bands with the dark subspace, as they can be reproduced with identical Bloch bands computation for dark-state-projected model H_2. The vertical lines originate from E_- bright states and are modeled by the Hamiltonian

$$H_{B_-} = -\frac{\hbar^2}{2m_a}\frac{d^2}{dx^2} + E_-(x). \tag{34}$$

Energy levels that can be traced to $E_+(x) \gg 0$ are absent in the figure. This channel does not have any energy levels at energies close to zero; however, its eigenstates can be coupled to dark states off-resonantly.

―――――――
[2]In this work we have used the standard SCIPY diagonalization function EIGS.

The dark subspace bands have two values, which results from the fact that the coefficients of $A(x)$ and A^2 as in (12) are of period $\lambda_L/2$ and the Bloch theory applied to Fig. 3 assumes a twice larger lattice period of λ_L, the natural period of Eq. (1). Complementary results from the H_2 model could be obtained from Bloch theory with lattice period $\lambda_L/2$ and a larger Brillouin zone $\mathrm{BZ}_2 = [-2\pi/\lambda_L, 2\pi/\lambda_L]$. This would yield dark-only Bloch eigenfunctions of the form

$$(B_D)_q^\alpha = e^{iqx}\big[b_{D_1}(x)|D_1(x)\rangle + b_{D_2}(x)|D_2(x)\rangle\big]$$
$$\equiv e^{iqx}\big[b_{D_1}(x), b_{D_2}(x)\big]^T, \tag{35}$$

where $q \in \mathrm{BZ}_2$ and b_* are $\lambda_L/2$ periodic. We note that the above vector, when reexpressed in $|g_1\rangle$, $|g_2\rangle$, $|g_3\rangle$, and $|e\rangle$, is only λ_L periodic just like $|D_1(x)\rangle$ and $|D_2(x)\rangle$. The four-channel computation for large $\|\mathbf{\Omega}\|$ yields a good approximation of the above. For quasimomenta $q, q' \in \mathrm{BZ}_2$, $q \in \mathrm{BZ}_1$, such that $|q - q'| = 2\pi/\lambda_L$, the λ_L-periodic Bloch theory treatment of the full H ascribes them both to a single $q \in \mathrm{BZ}_1$. Such folding has already appeared for a special case of the Λ system (see [10]) and is not unique to the tripod configuration; it is a simple consequence of the mismatch between the dark-state lattice constant and the period of the model.

Couplings due to $A(x)$ between dark states and the resonant E_- states lead to small avoided crossings [clearly visible in Fig. 3(a)]. Figure 3(b) illustrates the fact that for larger Ω_i the avoided crossings with the E_- bright state get narrower, indicating an even better isolation of the dark subspace. The improving separation between the dark subspace and the E_- bright band with increasing Ω_i is easily understood from the model (16). The avoided crossings appear between low-lying dark states and the highly excited E_- with the same $q \in \mathrm{BZ}_1$. Increasing $\|\mathbf{\Omega}\|$ pushes the E_- manifold towards more negative energies. As a result, for larger $\|\mathbf{\Omega}\|$ the wave vector describing freely moving E_- with approximately zero energy is more and more oscillating. This reduces the coupling to the dark-state Bloch vector via $A(x)$.

For a comparison we show also bands corresponding to the $a = 0$ case in Fig. 3(c). Here the dark state $|D_1\rangle$ is position independent [see (23)], the spectrum is a sum of that of a freely moving particle in channel D_1 [see Fig. 3(c)] and a D_2 particle sensing the presence of the potential (29). The two spectra intersect with each other with no avoided crossings forming between them. The bright-state line also does not couple to position-independent D_1 through $A(x)$ [Eq. (14)]. The avoided crossing prominent in Fig. 3(c) is between B_- and D_2 channel bands.

B. Dark band lifetime

Let us consider now the lifetime of different bands. When $\Gamma_e \neq 0$, in the Hamiltonian (2), the energies $E_\pm(x)$ of the bright-state channels (5) that appear in (11) and (12) are complex, in particular, $\mathrm{Im}E_\pm(x) = -\Gamma_e/4$ for $\Delta = 0$. The diagonalization of the model (2) focusing on the low-lying dark-state band reveals a strong q dependence of $\mathrm{Im}E_q^\alpha$ [as shown in Fig. 3(d)]. Here we assume $\Gamma_e = 1000E_R$ and the red shaded areas $\mathrm{Im}E_q^\alpha$ are multiplied by 50 to make them more visible. The q dependence for the Λ system was already

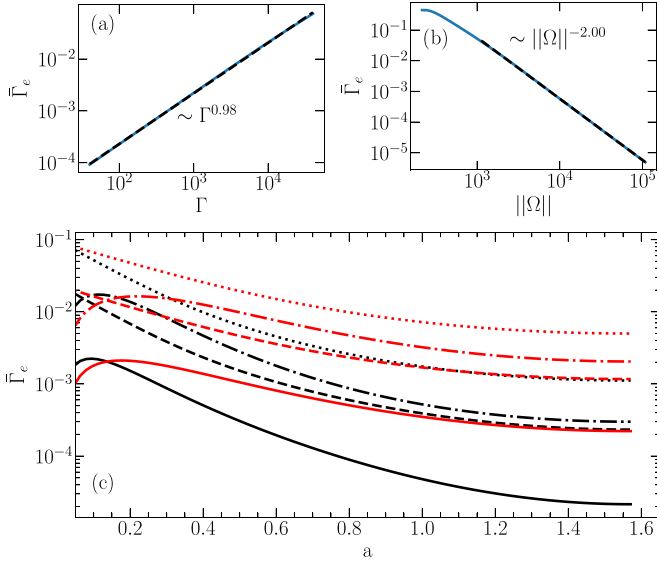FIG. 4. (a) The q-averaged decay rate $\bar{\Gamma}_e$ for ($\Omega_1 = 5000E_R$, $\Omega_2 = 2000E_R$, $\Omega_3 = 500E_R$) as a function of Γ_e for the second band. (b) Same as (a) as a function of $\|\boldsymbol{\Omega}\|$ for the same relative ratios of Ω_i and $\Gamma_e = 1000E_R$. (c) Plot of $\bar{\Gamma}_e$ as a function of a for $\Gamma_e = 1000E_R$ and two sets of $\Omega_i = (5000E_R, \Omega_2, 500E_R)$ for the first four bands. Black (darker) lines correspond to $\Omega_2 = 2000E_R$ and red (lighter) lines to $\Omega_2 = 1000E_R$. The bands are depicted in order as solid, dashed, dash-dotted, and dotted lines.

described in [10] and indirectly observed experimentally [14]. The total lifetime of the gas populating a certain band is approximated by the inverse of the q-averaged decay rate

$$\bar{\Gamma}_e = -\frac{2}{\text{vol}(\text{BZ}_1)} \int_{q \in \text{BZ}_1} \text{Im} E_q^\alpha \, dq. \tag{36}$$

Figure 4(a) shows the numerically obtained dependence of $\bar{\Gamma}_e$ on Γ_e for $\Omega_1 = 5000E_R$, $\Omega_2 = 2000E_R$, and $\Omega_3 = 500E_R$. Figure 4(b) shows the dependence on $\|\boldsymbol{\Omega}\|$ assuming a fixed ratio $\Omega_1 : \Omega_2 : \Omega_3 = 50 : 20 : 5$. Just like in the Λ system [10], one observes that $\bar{\Gamma}_e \propto \Gamma_e$ and $\|\boldsymbol{\Omega}\|^{-2}$.

A good approximation for $\text{Im}E_q^\alpha$ follows from the second-order perturbation theory arguments. The imaginary contribution to the energy of the dark-state Bloch function $(B_D)_q^\alpha(x)$ is

$$\text{Im}\Delta E_q^\alpha = -\sum_\beta \sum_{\sigma \in \pm} \frac{\Gamma_e}{2} \frac{\left| \langle (B_D)_q^\alpha | H_c | E_{q,\sigma}^\beta \rangle \right|^2}{\left[E_q^\alpha - \text{Re}(E_\sigma)_q^\beta \right]^2 + \frac{\Gamma_e^2}{4}}, \tag{37}$$

where $E_{\sigma,q}^\beta$ refer to bright-state eigenvectors in potentials $E_\sigma(x)$, $\sigma \in \pm$, with the same quasimomentum q. The H_c in (37) contains all the nondiagonal terms in the Hamiltonian (16). For the vast majority of states indexed by β, the Γ_e^2 term in the denominator may be neglected. Moreover, the sum is dominated by bright states $E_-(x)$ with energy close to $\max E_-(x) \propto \|\boldsymbol{\Omega}\|$ and bright states of $E_+(x)$ with energy close to $\min E_+(x) \propto \|\boldsymbol{\Omega}\|$. This qualitatively explains the observed dependence on Γ_e and $\|\boldsymbol{\Omega}\|$.

The coupling in the numerator of (37) depends on the $A(x)$ terms in (12). It is greatly increased if the coefficients of A responsible for the coupling of the dark state to the bright
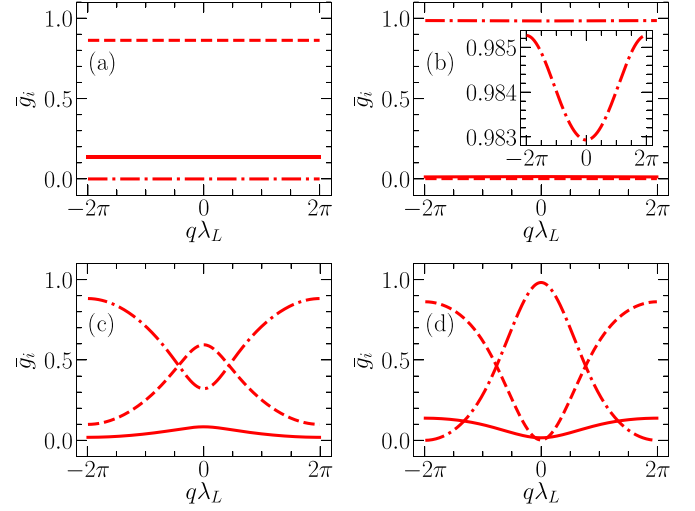

FIG. 5. Decomposition of Bloch states in BZ_2 into $|g_i\rangle$, where solid, dashed, and dash-dotted lines correspond to $i = 1, 2, 3$, respectively. Shown for (a) and (b) $a = 0$ and (c) and (d) $a = 0.435$ are (a) and (c) the lowest bands and (b) and (d) the first-excited bands. The inset in (b) shows the weak dependence of $|g_i\rangle$ in this panel using $|g_3\rangle$ as an example.

states are sharply peaked and large, as it happens in the $a \to 0$ limit, leading then to larger losses as shown in Fig. 4(c). Already $a = 0.435$ offers an order of magnitude longer lifetime than the Λ system case, $a = 0$. We also note that the ratio of $\Omega_1 : \Omega_2 : \Omega_3$ strongly affects the expected lifetime, particularly for large a. Figure 4(c) presents the simulated $\bar{\Gamma}_e$ for the first four bands for $\boldsymbol{\Omega} = (5000E_R, 2000E_R, 500E_R)$ (black lines) and $\boldsymbol{\Omega} = (5000E_R, 1000E_R, 500E_R)$ (red lines). Reducing the ratio $\Omega_2 : \Omega_3$ from 4 to 2 results in an order of magnitude shorter lifetime for large $a \approx \pi/2$.

C. Spin decomposition of Bloch bands

Let us discuss the decomposition of Bloch eigenvectors into atomic states $|g_1\rangle$, $|g_2\rangle$, $|g_3\rangle$, and $|e\rangle$. We use again our exemplary set of parameters $\boldsymbol{\Omega} = (5000E_R, 2000E_R, 500E_R)$ for illustration, taking also $\Gamma_e = 0$. Figure 5 shows the averages $\bar{g}_i = \int_0^{\lambda_L} |\langle B_q^\alpha | g_i \rangle|^2$ for different quasimomenta within the first two bands of the $a = 0$ and $a = 0.435$ systems.

For $a = 0$ the lowest "band" is actually a portion of the parabolic energy dependence of a freely moving particle. It forms a closed band as soon as $a \neq 0$. The $\bar{g}_i$ are in that case constant and given by the constant coefficients of Eq. (23). For the first-excited band, that is, the lowest band in the D_2 channel, the dependence on q is very small [Fig. 5(b)]. When $a \neq 0$ is increased towards the final value $a = 0.435$ the well-defined bands are formed, as in Fig. 3(a). Different parts of each band intersect other energy levels, experiencing avoided crossings in different ways. For example, the D_1 and D_2 channels at energy close to $1E_R$ for $q = 0$ in Fig. 3(c) experience transition through the avoided crossing before the well-separated bands in Fig. 3(a) are formed. At the same time the energy levels at $q = \pm\pi/\lambda_L \in \text{BZ}_1$ remain nearly unaffected by other energy levels. This is the reason for the observed strong dependence on q of decompositions $\bar{g}_i$ in

Figs. 5(c) and 5(d) for $a = 0.435$. Specifically, one can observe that decomposition into $\bar{g}_i$ of the first-excited band for $q = 0 \in \text{BZ}_2$ resembles the decomposition of the D_2 channel in Fig. 5(b) and for $q = \pm 2\pi/\lambda_L \in \text{BZ}_2$ that of D_1 in Fig. 5(a). At the same time the lowest band shows a strong dependence of $\bar{g}_i$ on q which however does not approximate D_1 or D_2 for any q.

The variation of the overlap of Bloch vectors on $|g_1\rangle$, $|g_2\rangle$, and $|g_3\rangle$ within the same band is directly observable. Consider a bosonic, noninteracting gas cooled down to the least energetic state of the band. Denote the quasimomentum of such a state by q_0. If an extra potential $H_{\text{tilt}} = -Fx$ is added (see [20]) to the Hamiltonian (1), then a steady drift of the quasimomentum $q(t) = q_0 + Ft/\hbar$ occurs, allowing one to reach the desired value of q by controlling the application time of H_{tilt}. The value of $F\lambda_L$ should be much smaller than the energy gap to other bands, to prevent populating them. The spin decomposition can be studied by turning off the lasers responsible for Rabi frequencies Ω_i and splitting the atomic cloud in the $|g_1\rangle$, $|g_2\rangle$, and $|g_3\rangle$ components by a magnetic-field gradient. The response of the tripod system to the gradient H_{tilt} would form a coherent time-dependent transfer of populations of atomic states $|g_1\rangle$, $|g_2\rangle$, and $|g_3\rangle$, a feature which is easily measurable.

IV. TIGHT-BINDING MODEL

A tight-binding model conveniently describes movement of the particles populating a particular band. We describe first the construction of the Wannier functions in analogy to the textbook Wannier function calculation for a cosine-squared optical lattice [21–23].

A. Construction of Wannier functions in two-dimensional dark subspace

We start with the basis of all the dark-state Bloch functions $\{(B_D)_q^\alpha : q \in \text{BZ}_2\}$ for a particular band α of H_2. Then the Wannier function can be expressed as

$$W_n^\alpha(x) = N \int_{q \in \text{BZ}_2} (B_D)_q^\alpha(x) e^{i\theta_{q,n}} dq, \qquad (38)$$

where the index n denotes localization over the nth lattice site, $x_n = x_0 + n\lambda_L/2$, and N ensures that $\int_{\mathbb{R}} |W_n^\alpha(x)|^2 dx = 1$. The functional dependence of phases $\theta_{q,n}$ on q has to be chosen to localize the W_n^α. To find it, we adapt the method by Kivelson [22]. The H_2 Hamiltonian is considered under periodic boundary conditions in a box of a sufficient total length L. This discretizes the Brillouin zone $\text{BZ}_2 \to [0, 2\pi/L, \ldots, 4\pi/\lambda_L)$. We construct the $L \times L$ matrix

$$M_{q,q'} = \langle (B_D)_q^\alpha | e^{2\pi ix/L} | (B_D)_{q'}^\alpha \rangle, \quad q, q' \in \text{BZ}_2. \qquad (39)$$

Its eigenvalues are complex phases of the type $\exp[(2\pi ix_n)/L]$, which determines x_0. The corresponding eigenvector then defines the values of $\theta_{q,n}$ that localize W_n^α around the location x_n. We have verified that the obtained Wannier functions are exponentially localized around x_n, as expected for this procedure [22]. It is also worth noting that by using this method Wannier functions can be computed directly within λ_L-periodic Bloch theory ($q \in \text{BZ}_1$) by

including both branches of a folded band while computing the matrix elements of (39).

For a single-channel problem with a periodic potential, one can calculate a single Wannier function, e.g., $W_0(x)$, and then use a discrete translation $W_n(x) := W_0(x - (x_n - x_0))$ to complete the basis. For the tripod system this is also a possibility, but special care should be taken when applying translation to $W_0^\alpha(x)$ given by Eq. (38) when expressed in the $|g_i\rangle$ and $|e\rangle$ basis. Indeed, if we expand $W_n^\alpha(x)$ in the $|D_i(x)\rangle$ basis

$$W_0^\alpha(x) = w_1(x)|D_1(x)\rangle + w_2(x)|D_2(x)\rangle, \qquad (40)$$

then one can shift the $w_i(x)$ functions only and resum the $W_n(x)$ to obtain

$$W_n^\alpha(x) = w_1(x - n\lambda_L/2)|D_1(x)\rangle + w_2(x - n\lambda_L/2)|D_2(x)\rangle. \qquad (41)$$

Instead one might attempt to translate the entire $W_0^\alpha(x)$, obtaining

$$w_1(x - n\lambda_L/2)|D_1(x - n\lambda_L/2)\rangle$$
$$+ w_2(x - n\lambda_L/2)|D_2(x - n\lambda_L/2)\rangle \neq W_n^\alpha(x). \qquad (42)$$

As $|D_i(x)\rangle$ are only λ_L periodic, both approaches are not equivalent for odd n. The former approach leading to (41) is a proper one, as it corresponds to a shift of the coefficients of the Wannier function by the Hamiltonian H_2 lattice constant for a single-valued band defined by H_2 with a BZ of BZ_2. We have verified that for odd n, W_n^α translated as in (42) is not orthogonal to $W_0^\alpha(x)$. The properties of Wannier functions are discussed further in Sec. IV D, after constructing the tight-binding Hamiltonian description.

B. Hopping amplitudes

The Hamiltonian H_2, restricted to band α when expressed in the basis $W_n^\alpha(x)$, transforms to

$$H_{\text{hopp},\alpha} = -\sum_{n,m} J_{nm}^{\alpha\alpha} (\hat{a}_n^\alpha)^\dagger \hat{a}_m^\alpha + \text{H.c.}, \qquad (43)$$

where

$$J_{nm}^{\alpha\alpha} = -\int dx (W_n^\alpha)^\dagger(x) H_2(x) W_m^\alpha(x)$$
$$= -\frac{1}{\text{vol}(\text{BZ}_2)} \int_{\text{BZ}_2} e^{i(m-n)q\lambda_L/2} E_q^\alpha dq. \qquad (44)$$

The second equality is true assuming that the global phase factors of $W_n^\alpha(x)$ are defined by (41). The hopping amplitudes depend only on the distance between sites n and m so one can simplify the notation by defining

$$J_{|n-m|}^\alpha := J_{n,m}^{\alpha\alpha}. \qquad (45)$$

The hopping amplitudes (referred to simply as hoppings later on) may be directly calculated from their definition (44) using previously determined Wannier functions. Their exponential tail requires, however, special care for accurate determination of J_i^α, which is important, in particular, for $i > 1$. However, the hoppings J_i^α can be read from the band

energies, for $q \in \mathrm{BZ}_2$:

$$E_q^\alpha = E_0 - 2J_1^\alpha \cos\left(\frac{q\lambda_L}{2}\right) - 2J_2^\alpha \cos\left(\frac{2q\lambda_L}{2}\right) - \cdots .$$

$$(46)$$

Calculation directly in the $|g_i\rangle$ and $|e\rangle$ basis followed by band unfolding suffices to determine J_i^α as well. As the J_i are defined with respect to $q \in \mathrm{BZ}_2$, a mistake in the unfolding of $q \in \mathrm{BZ}_1$ would lead to a sign flip of the J_i with an odd i. The Bloch vectors obtained in the four-channel calculation can be projected back onto the $(|D_1(x)\rangle, |D_2(x)\rangle)$ space. The quasiperiodicity of the coefficients

$$b_{D_i}\left(\frac{x + \lambda_L}{2}\right) = \exp\left(\frac{iq\lambda_L}{2}\right)b_{D_i}(x), \qquad (47)$$

allows us to distinguish the two Bloch states $q, q' \in \mathrm{BZ}_2$, $|q - q'| = 2\pi/\lambda_L$, which correspond to the same point in BZ_1.

Unfortunately, the band unfolding by assigning $q', q \in \mathrm{BZ}_2$ is gauge dependent. Applying Eq. (47) uses a particular gauge during projection on $|D_i(x)\rangle$. As a result, when two eigenvectors for a particular $q \in \mathrm{BZ}_1$ are being relabeled by $q, q' \in \mathrm{BZ}_2$, $|q - q'| = 2\pi/\lambda_L$, the assignment of q, q' is reverse for D_i as in Eqs. (20) and (21) and D_i as in Eqs. (26) and (27). This means that the dependence on q of the quasienergy E_q^α present in Eq. (46) differs by a translation by $2\pi/\lambda_L$ and a sign flip in J_n: $J_n^\alpha \to J_n^\alpha(-1)^n$. The ambiguity of signs of J_i^α is not in conflict with the definition of J_i^α by means of the Wannier functions (44). It is fully recovered when the J_n^α are computed from Eq. (44) in both gauges.

We follow the gauge choice given by Eqs. (20) and (21) and calculate the tunnelings for low-lying (and long-living) bands. Again we discuss similar parameter values as before, i.e., $\mathbf{\Omega} = (5000, 2000, 500)E_R$. Consider first the lowest band taking a form as in standard Bose-Hubbard (compare Fig. 3). Not surprisingly $|J_2| \ll J_1$ for most of the values of the phase shift parameter a; thus nearest-neighbor hopping dominates. Interestingly, however, J_1 changes sign when a is varied [compare Fig. 6(a)], which allows for realization of frustration as discussed in Sec. IV C.

In Figs. 6(b) and 6(c) we show the values of J_i^α as a function of a for the first-excited, almost flat, band (compare Fig. 3) that results in an unusual relation between J_1 and longer distance hopping amplitudes. For $a < 0.2$ or $a > 0.45$, for this band, the amplitudes for long-distance hopping J_i with $i > 3$ are non-negligible, indicating that the tight-binding approach may not be the best choice in such a case. However, for $a \in [0.2, 0.45]$ only J_1, J_2, and J_3 can be considered for an accurate tight-binding model. The next-nearest hopping J_2 is larger then the nearest-neighbor amplitude J_1 and larger than the next-to-next-nearest-neighbor amplitude J_3. Only for $a \approx 0.1$ do J_1 and J_2 become comparable. Around $a = 0.435$ a special situation occurs as $J_1 \approx 0$. This is in agreement with band structures in Fig. 3, where the second band seems to be "single valued" at the scale of the figure.

Figure 6(d) shows a similar calculation of hopping amplitudes for the excited band, but for the ratio of $\Omega_1:\Omega_2:\Omega_3 = 50:40:5$. The same configurations of amplitudes J_i occur in a different range of the phase shift a parameter. The correspond-
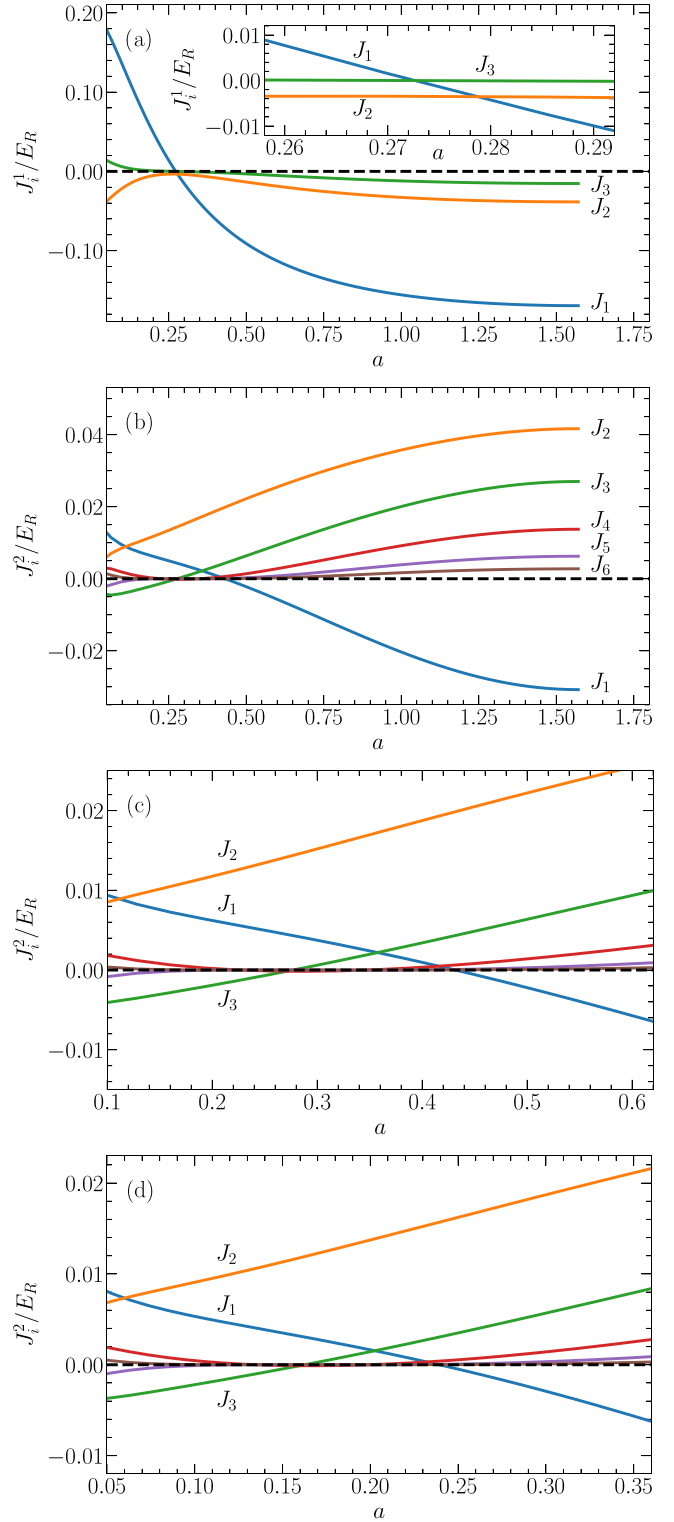

FIG. 6. Different hopping amplitudes J_i^α as a function of a, the relative phase difference between $\Omega_1(x)$ and $\Omega_2(x)$. (a) Ground band $\alpha = 1$ for $\Omega_1:\Omega_2:\Omega_3 = 50:20:5$. (b) Same systems as in (a) but in the first-excited band $\alpha = 2$. (c) Magnification of (b) with a narrower range of a. (d) Analogous range of a but for $\Omega_1:\Omega_2:\Omega_3 = 50:40:5$.

ing interval for a is [0.1,0.22]. Its location and size depend approximately linearly on the ratio $\Omega_3:\Omega_2$, as long as $\Omega_2 < \Omega_1$ and $\Omega_2/\Omega_3 \gg 1$. When $\Omega_2/\Omega_3 \approx 1$ the region of interest
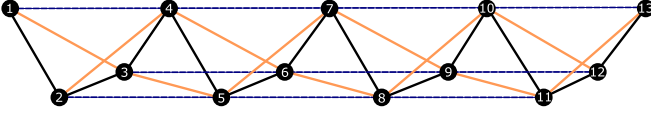
FIG. 7. Mapping of a 1D chain with NN, NNN, and NNNN tunnelings into a tetrahedral linear compound with nearest-neighbor tunnelings only. Along dashed blue lines J_3 tunnelings occur, orange lines correspond to J_2, and black connections yield the nearest-neighbor terms J_1.

does not exist (naive interpolation puts it for $a > \pi/2$). When $\Omega_2 > \Omega_1$ the roles of Ω_1 and Ω_2 are reversed.

C. Frustration

It is well known that a one-dimensional (1D) spin-$\frac{1}{2}$ chain with J_1 (NN) and J_2 (NNN) interactions may exhibit frustration [24], a situation in which it is not easy to satisfy energetic minimalization of all the possible bonds [25]. Such a chain maps onto a nonpartite triangular ladder in which for negative tunnelings J_1 and J_2 kinetic frustration occurs ([26] reviews the physics of periodically driven systems that enable a change of sign of the tunneling matrix elements; see also [27]). In our situation the sign of J_1 (or any J_i for odd i) can be inverted by a gauge transformation (reverting to the sign of the every second Wannier function). It is thus more interesting that for the lowest band J_2 becomes negative (antiferromagnetic). For most a values J_1 dominates, making frustration difficult to observe. However, since J_1 changes sign [around $a = 0.275$ for the chosen values of Ω_i; see Fig. 6(a)] it becomes small and comparable to J_2 for nearby a values, leading to a quite standard frustrating system. Note that a change of sign of J_1 in triangular lattices was realized via periodic lattice shaking (see [26,27] and references therein); here no additional shaking is needed and frustrating conditions are realized by changing the phase mismatch a.

The situation is equally interesting for the first-excited band. Here (compare Fig. 6) both the NN J_1 and NNNN J_3 may change sign depending on the a value, while J_2 remains positive and large. Consider first the simplest situation when we adjust a such that J_3 vanishes. The system maps to a triangular ladder with J_2 positive and regardless of the sign of J_1 no frustration occurs. This is again a manifestation of the fact that the change of sign of every second Wannier functions is just a gauge transformation that changes the sign of J_{2i+1} leaving the physics unaltered.

In the presence of J_3 the models becomes less obvious. The mapping on the triangular ladder does not work anymore. Instead, one can map a 1D chain into a three-dimensional tetrahedral linear compound as depicted in Fig. 7. Such a representation allows for a better visualization of the competition between different hopping terms. Now it is easy to see that if the signs of J_1 and J_3 are different, the system will be frustrated as one cannot minimize energetically the $i, i+1$ and $i, i+3$ bonds. On the other hand, in the interval of a values where J_1 and J_3 are of the same sign, no kinetic frustration occurs.
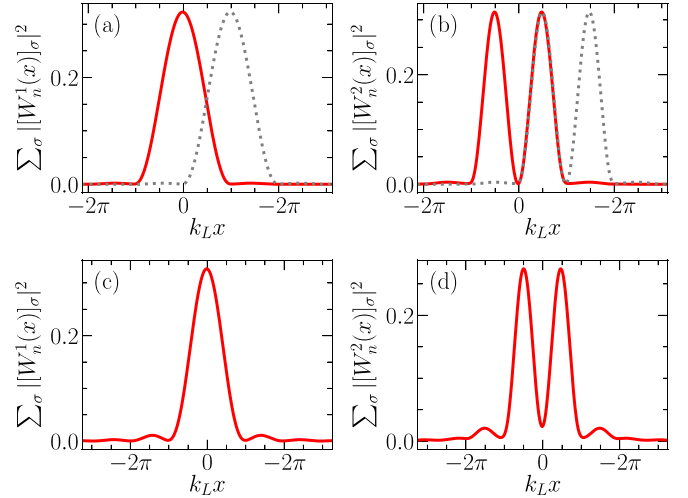

FIG. 8. Sums of amplitude moduli squared of all components e, g_1, g_2, and g_3 of Wannier functions for (a) and (c) the lowest band and (b) and (d) the first-excited band and for $\Omega_i = (5000, 2000, 500)E_R$ and (a) and (b) $a = 0.435$ and (c) and (d) $a = 1.3$. Gray dotted lines depict the same Wannier functions but in an adjacent lattice site. Orthogonality of heavily overlapping Wannier functions is possible due to the interplay of phases of individual bare atomic components components g_1, g_2, and g_3.

D. Properties of Wannier functions

In light of highly nonstandard relations between J_1, J_2, and J_3 hopping amplitudes (Sec. IV B) it is instructive to inspect spatial profiles of Wannier functions of the tripod system. Again assume $\mathbf{\Omega} = (5000E_R, 2000E_R, 500E_R)$ as an example. Figure 8 shows the total density $\|W_n^\alpha\|^2$ for the Wannier functions. Figures 8(a) and 8(c) show the Wannier function for the lowest dark-state band for $a = 0.435$ and $a = 1.3$, respectively. The notable feature is a nonvanishing overlap of densities of neighboring Wannier functions (they remain of course orthogonal to each other). For a large a additional modulation shows, indicating poorer confinement which corresponds well with large values of long-range hopping $J_{i>3}$. For the first-excited band Figs. 8(b) and 8(d) show again the $a = 0.435$ and $a = 1.3$ cases. The second band shows Wannier functions that are bimodal and have a total width of approximately λ_L. Despite that, the $\lambda_L/2$-displaced Wannier functions are mutually orthogonal. This is possible only because the Wannier functions can alter decomposition into separate g_1, g_2, and g_3 in a position-dependent way. When calculating the inner product of W_n^α and W_{n+1}^α the result is zero only after the summation over $\sigma \in g_1, g_2, g_3$. This is not possible in a scalar Wannier function for a standard optical potential.

Standard integrals describing two-particle interaction in Hubbard-type models are often of the type

$$U = \int \bar{W}_n(x)\bar{W}_m(x')V(x - x')W_o(x')W_p(x)dx\,dx'. \quad (48)$$

For the first-excited band the Wannier functions W_n and W_{n+1} significantly overlap, allowing the above integral to yield a

large value of U even for non-on-site processes. This potentially makes construction of discrete models with long-range interaction much easier without the need to use, e.g., dipolar interactions. This correlates well with with nonstandard relations between J_1^α, J_2^α, and J_3^α, which allow also for long-range hopping.

V. SUMMARY AND OUTLOOK

In this work a four-level system in tripod configuration hosting two dark states was presented. The position dependence of the dark state was set by the position dependence of Rabi frequencies $\Omega_i(x)$. This constraint creates periodic gauge-field-like potentials that give rise to a band structure with well-separated bands. In contrast to the conceptually similar case of the three-level system in the Λ configuration, the lifetime of the gas populating the bands can be substantially increased. The controlling parameter is a, the phase difference between two lasers implementing the Ω_1 and Ω_2 couplings. The band structure is characterized by highly nonstandard relations between hopping amplitudes and nearest-, next-nearest-, next-to-next-nearest-neighbor lattice sites, allowing for efficient long-range hopping. This is reflected in the nonstandard shape of Wannier functions for the appropriate bands that are supported at two neighboring unit cells.

Note added in proof. Recently, we became aware of a recent work of Gvozdiovas *et al.* [28] that also considers a similar tripod configuration for optical lattice creation. We believe that our choice of parameters minimizes the population of bright states (which makes such a lattice more stable than for the choice in [28]).

ACKNOWLEDGMENTS

APPENDIX A: DIFFERENT GAUGE CHOICE

It is natural to ask how other choices of the dark-state basis compare to the one discussed above. A general different possible basis choice for the dark-state subspace is given by a position-dependent two-dimensional unitary transformation

$$(|D_1(x)\rangle, |D_2(x)\rangle) \rightarrow U_2(x)(|D_1(x)\rangle, |D_2(x)\rangle), \quad \text{(A1)}$$

by angle $\alpha(x)$. Such a transformation preserves the overall Hamiltonian form with $A(x)$ transformed as

$$A \rightarrow U(x)AU^\dagger(x) - i\hbar \frac{\partial U(x)}{\partial x} U^\dagger(x), \quad \text{(A2)}$$

where $U(x)$ is a four-dimensional extension of $U_2(x)$ including the transformation of the bright states (by phase factors). To preserve $A_{ii} = 0$, $i < 3$, we can use $U_2(x) = \exp[i\sigma_y \alpha(x)]$. The extra freedom to pick $\alpha(x)$ unfortunately does not allow for nullification of nondiagonal terms of $A(x)$ (see Appendix B).

Features such as the height and location of $(A^2)_{11}$ and $(A^2)_{22}$ peaks and the spatial dependence of terms $(A^2)_{12}$ and
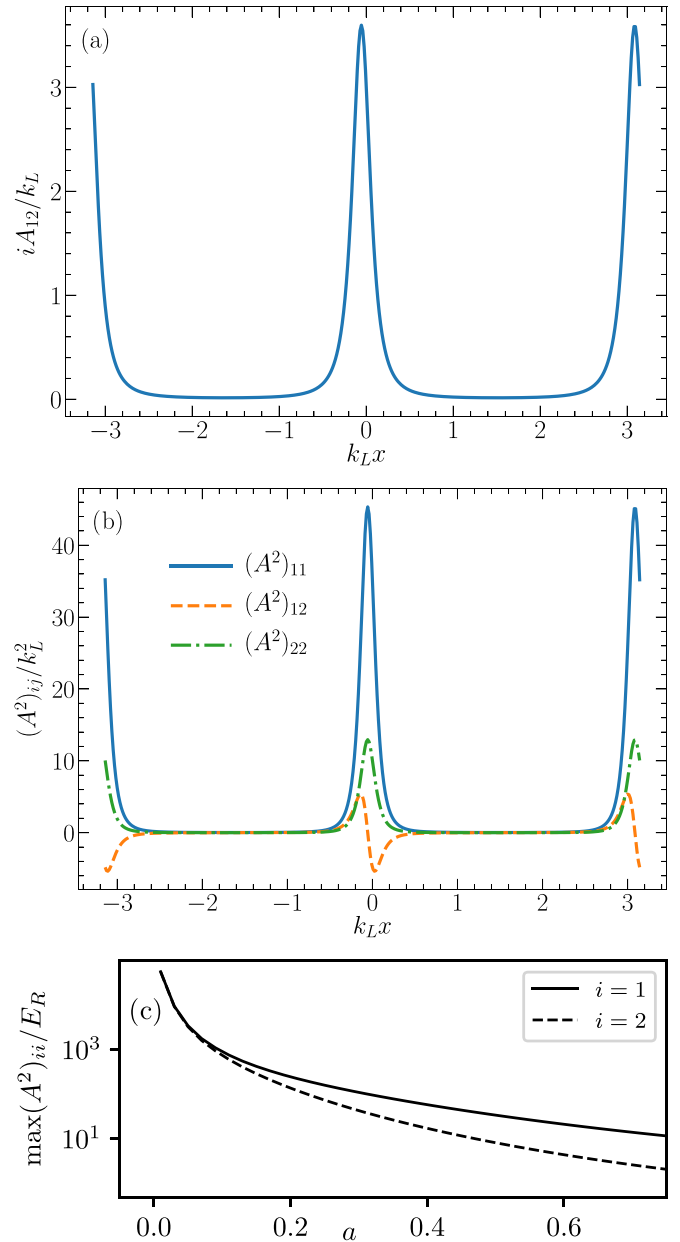

FIG. 9. Spatial dependence of elements of matrices $A(x)$ and $A^2(x)$, determined assuming the problematic dark-state definition in Eqs. (26) and (27) for Ω_1:Ω_2:$\Omega_3 = 50$:20:5 and $a = 0.435$; (a) $A_{12}(x)$, the only nonzero element of A as given by (A3); (b) elements of $A^2(x)$, i.e., $(A^2)_{11}$, $(A^2)_{22}$, and $(A^2)_{12}$; and (c) dependence of peak height in $(A^2)_{11}$ and $(A^2)_{22}$ on a and divergent behavior at $a \to 0$.

$(A^2)_{22}$ are strongly gauge dependent. To illustrate this we consider an alternative gauge choice. Instead of using dark states in Eqs. (20) and (21) we use Eqs. (26) and (27) as a basis for determination of the potential $A(x)$. Figure 9 shows the gauge potentials in that case. Due to analytical simplicity of Eqs. (26) and (27), one can work out the formulas for the $A(x)$. They are

$$A_{11}(x) = A_{22}(x) = 0,$$

$$A_{12}(x) = -ik_L \frac{\Omega_1\Omega_2\Omega_3 \sin a}{\Xi_1^2(x)\Xi_2(x)},$$

$$(A^2)_{11}(x) = k_L^2 \left(\frac{\Omega_1 \Omega_2 \sin a}{\Xi_1^2(x)} \right)^2,$$

$$(A^2)_{12}(x) = -k_L^2 \frac{\Omega_1 \Omega_2 \Omega_3 \chi(x) \sin a}{\Xi_1^2(x) \Xi_2^3(x)},$$

$$(A^2)_{22}(x) = k_L^2 \left[\left(\frac{\Omega_1 \Omega_2 \Omega_3 \sin a}{\Xi_1^2(x) \Xi_2(x)} \right)^2 + \left(\frac{\Omega_3 \chi(x)}{\Xi_1(x) \Xi_2^2(x)} \right)^2 \right], \tag{A3}$$

where

$$2\Xi_1^2(x) = \left(\Omega_1^2 + \Omega_2^2 \right) - C \cos(2k_L x + b),$$

$$\Xi_2^2(x) = \Omega_3^2 + \Xi_1^2(x),$$

$$2\chi(x) = C \sin(2k_L x + b),$$

$$C = \sqrt{\Omega_1^4 + \Omega_2^4 + 2\Omega_1^2 \Omega_2^2 \cos 2a},$$

$$\sin b = \frac{\Omega_2^2 \sin 2a}{C}. \tag{A4}$$

In this case the gauge potentials differ qualitatively from the ones in Fig. 2. First the potential maxima of $(A^2)_{11}$ and $(A^2)_{22}$ coincide and $(A^2)_{22}$ is nearly zero far from potential peaks. In the gauge choice defined by Eqs. (20) and (21) the potential $(A^2)_{11}$ features a series of narrow peaks that are located between the peaks of $(A^2)_{22}$, shifted by $\lambda_L/4$.

Another distinct feature of the choice in Eqs. (26) and (27) is divergence of height of peaks of $(A^2)_{11}$ as $a \to 0$ [see Fig. 9(c)]. This is in stark contrast to the case of Fig. 2, where $(A^2)_{11} \to 0$. This straightforwardly follows from Eq. (26). This is because for $x = 0$ and $x = -a$ the $|D_1(x)\rangle$ is $|g_2\rangle$ and $|g_1\rangle$, respectively. This implies rapid variation of $|D_1(x)\rangle$ and in turn divergent $A_{11}^2(x)$ [see Eq. (28)].

APPENDIX B: FAILURE TO ZERO A_{12} BY THE GAUGE TRANSFORMATION

Using the gauge freedom, one could hope to vanish all elements of A_{KL} in the dark subspace. Then the dark-subspace Hamiltonian would simplify to

$$H = \frac{P^2}{2m} + \frac{(A^2)_{2 \times 2}}{2m}. \tag{B1}$$

We consider a system where $\tilde{\Delta} = 0$ and Ω_i are real giving, $A_{11} = A_{22} = 0$. We choose an arbitrary position-dependent

basis of $\mathbf{d}_1(x)$ and $\mathbf{d}_2(x)$. The convenient choice is

$$\mathbf{d}_1(x) = \hat{\Omega} \times \frac{\hat{\Omega}'}{\|\hat{\Omega}'\|},$$

$$\mathbf{d}_2(x) = -\frac{\hat{\Omega}'}{\|\hat{\Omega}'\|}, \tag{B2}$$

where $\hat{\Omega} = \boldsymbol{\Omega}/\|\boldsymbol{\Omega}\|$. The equation $A_{12} = 0$ implies

$$\mathbf{D}_1' \times \boldsymbol{\Omega} = 0,$$

$$\mathbf{D}_2' \times \boldsymbol{\Omega} = 0. \tag{B3}$$

We see that there is still residual gauge freedom; we can rotate the basis by any position-independent rotation matrix. This freedom is well captured when we reformulate our problem. We express $\mathbf{D}_i$ as a position-dependent rotation of $\mathbf{d}_i$:

$$\begin{pmatrix} \mathbf{D}_1(x) \\ \mathbf{D}_2(x) \end{pmatrix} = \begin{pmatrix} \cos[\alpha(x)] & -\sin[\alpha(x)] \\ \sin[\alpha(x)] & \cos[\alpha(x)] \end{pmatrix} \begin{pmatrix} \mathbf{d}_1(x) \\ \mathbf{d}_2(x) \end{pmatrix}. \tag{B4}$$

After some algebra, we can write the final equation for $\alpha(x)$:

$$\alpha'(x) = \frac{\hat{\Omega} \cdot (\hat{\Omega}' \times \hat{\Omega}'')}{\|\hat{\Omega}'\|^2} = \det(\hat{\Omega}, \hat{\Omega}', \hat{\Omega}'')/\|\hat{\Omega}'\|^2. \tag{B5}$$

The solution is unique up to a constant, which reflects the residual gauge freedom. In this gauge

$$A = \frac{i\hbar}{\sqrt{2}} \|\hat{\Omega}'\| \begin{pmatrix} 0 & 0 & \sin\alpha & \sin\alpha \\ 0 & 0 & -\cos\alpha & -\cos\alpha \\ -\sin\alpha & \cos\alpha & 0 & 0 \\ -\sin\alpha & \cos\alpha & 0 & 0, \end{pmatrix}, \tag{B6}$$

and

$$A^2 = \hbar^2 \|\hat{\Omega}'\|^2 \begin{pmatrix} \sin^2\alpha & -\sin\alpha\cos\alpha & 0 & 0 \\ -\sin\alpha\cos\alpha & \cos^2\alpha & 0 & 0 \\ 0 & 0 & \frac{1}{2} & \frac{1}{2} \\ 0 & 0 & \frac{1}{2} & \frac{1}{2} \end{pmatrix}. \tag{B7}$$

There is however one problem: Although $\alpha'(x)$ is essentially periodic for periodic $\boldsymbol{\Omega}$, the solution $\alpha(x)$ may not be, when $\int_{\text{period}} dx \, \alpha'(x) \neq n\pi$, $n \in \mathbb{Z}$,. Then, for $\boldsymbol{\Omega}(x) = \boldsymbol{\Omega}(x + \lambda)$, Eq. (B4) implies that $\mathbf{D}_1(x)$ and $\mathbf{D}_2(x)$ are aperiodic functions of x. This aperiodicity translates back to the remaining terms of $A(x)$ via (B6), which makes it impossible to directly apply Bloch theory.

[1] D. Jaksch, C. Bruder, J. I. Cirac, C. W. Gardiner, and P. Zoller, Phys. Rev. Lett. **81**, 3108 (1998).

[2] M. Greiner, O. Mandel, T. Esslinger, T. W. Hänsch, and I. Bloch, Nature (London) **415**, 39 (2002).

[3] M. Lewenstein, A. Sanpera, and V. Ahufinger, *Ultracold Atoms in Optical Lattices: Simulating Quantum Many-Body Systems* (Oxford University Press, Oxford, 2012).

[4] O. Dutta, M. Gajda, P. Hauke, M. Lewenstein, D.-S. Luehmann, B. A. Malomed, T. Sowiński, and J. Zakrzewski, Rep. Prog. Phys. **78**, 066001 (2015).

[5] N. R. Cooper, J. Dalibard, and I. B. Spielman, Rev. Mod. Phys. **91**, 015005 (2019).

[6] O. Boada, A. Celi, J. I. Latorre, and M. Lewenstein, Phys. Rev. Lett. **108**, 133001 (2012).

[7] A. Celi, P. Massignan, J. Ruseckas, N. Goldman, I. B. Spielman, G. Juzeliūnas, and M. Lewenstein, Phys. Rev. Lett. **112**, 043001 (2014).

[8] D. Suszalski and J. Zakrzewski, Phys. Rev. A **94**, 033602 (2016).

[9] M. Lohse, C. Schweizer, H. M. Price, O. Zilberberg, and I. Bloch, Nature (London) **553**, 55 (2018).

[10] M. Łącki, M. A. Baranov, H. Pichler, and P. Zoller, Phys. Rev. Lett. **117**, 233001 (2016).

[11] F. Jendrzejewski, S. Eckel, T. G. Tiecke, G. Juzeliūnas, G. K. Campbell, L. Jiang, and A. V. Gorshkov, Phys. Rev. A **94**, 063422 (2016).

[12] J. Larson and J.-P. Martikainen, Phys. Rev. A **78**, 063618 (2008).

[13] J. Larson and J.-P. Martikainen, Phys. Rev. A **80**, 033605 (2009).

[14] Y. Wang, S. Subhankar, P. Bienias, M. Łącki, T.-C. Tsui, M. A. Baranov, A. V. Gorshkov, P. Zoller, J. V. Porto, and S. L. Rolston, Phys. Rev. Lett. **120**, 083601 (2018).

[15] T.-C. Tsui, Y. Wang, S. Subhankar, J. V. Porto, and S. L. Rolston, Phys. Rev. A **101**, 041603(R) (2020).

[16] J. Ruseckas, G. Juzeliūnas, P. Öhberg, and M. Fleischhauer, Phys. Rev. Lett. **95**, 010404 (2005).

[17] J. Dalibard, F. Gerbier, G. Juzeliūnas, and P. Öhberg, Rev. Mod. Phys. **83**, 1523 (2011).

[18] Y.-J. Lin, K. Jiménez-García, and I. B. Spielman, Nature (London) **471**, 83 (2011).

[19] C. Hamner, Y. Zhang, M. A. Khamehchi, M. J. Davis, and P. Engels, Phys. Rev. Lett. **114**, 070401 (2015).

[20] M. Ben Dahan, E. Peik, J. Reichel, Y. Castin, and C. Salomon, Phys. Rev. Lett. **76**, 4508 (1996).

[21] W. Kohn, Phys. Rev. **115**, 809 (1959).

[22] S. Kivelson, Phys. Rev. B **26**, 4269 (1982).

[23] N. Marzari, A. A. Mostofi, J. R. Yates, I. Souza, and D. Vanderbilt, Rev. Mod. Phys. **84**, 1419 (2012).

[24] H.-J. Mikeska and A. K. Kolezhuk, in *Quantum Magnetism*, edited by U. Schollwöck, J. Richter, D. J. J. Farnell, and R. F. Bishop, Lecture Notes in Physics Vol. 645 (Springer, Berlin, 2004), pp. 1–83.

[25] H. T. Diep, *Frustrated Spin Systems* (World Scientific, Singapore, 2004).

[26] A. Eckardt, Rev. Mod. Phys. **89**, 011004 (2017).

[27] K. Sacha, K. Targońska, and J. Zakrzewski, Phys. Rev. A **85**, 053613 (2012).

[28] E. Gvozdiovas, P. Rackauskas, and G. Juzeliunas, arXiv:2105.15148.